Localized vegetation patterns, fairy circles, and localized patches in arid landscapes

D. Escaff,[1] C. Fernandez-Oto,[2] M. G. Clerc,[3] and M. Tlidi[2]
[1]*Complex Systems Group, Facultad de Ingeniería y Ciencias Aplicadas, Universidad de los Andes, Monseñor Alvaro del Portillo 12.455, Las Condes, Santiago, Chile*
[2]*Faculté des Sciences, Université Libre de Bruxelles (U.L.B.), C.P. 231, Campus Plaine, B-1050 Bruxelles, Belgium*
[3]*Departamento de Física, Universidad de Chile, Blanco Encalada 2008, Santiago, Chile*
(Received 25 November 2014; published 26 February 2015)

We investigate the formation of localized structures with varying widths in one- and two-dimensional systems. The mechanism of stabilization is attributed to strongly nonlocal coupling mediated by a Lorentzian type of kernel. We show that, in addition to stable dips found recently [see, e.g. Fernandez-Oto *et al.*, Phys. Rev. Lett. **110**, 174101 (2013)], there are stable localized peaks which appear as a result of strongly nonlocal coupling. We applied this mechanism to arid ecosystems by considering a prototype model of a Nagumo type. In one dimension, we study the front connecting the stable uniformly vegetated state to the bare one under the effect of strongly nonlocal coupling. We show that strongly nonlocal coupling stabilizes both—dip and peak—localized structures. We show analytically and numerically that the width of a localized structure, which we interpret as a fairy circle, increases strongly with the aridity parameter. This prediction is in agreement with published observations. In addition, we predict that the width of localized patch decreases with the degree of aridity. Numerical results are in close agreement with analytical predictions.

DOI: 10.1103/PhysRevE.91.022924 PACS number(s): 05.45.−a, 87.23.Cc, 87.18.Hf, 89.75.Kd

I. INTRODUCTION

Localized structures (LSs) in dissipative media have been observed in various fields of nonlinear science such as fluid dynamics, optics, laser physics, chemistry, and plant ecology (see recent overviews [1,2]). Localized structures consist of isolated or randomly distributed spots surrounded by regions in the uniform state. They may consist of dips embedded in the homogeneous background. They are often called spatial solitons, dissipative solitons, localized patterns, cavity solitons, or autosolitons, depending on the physical contexts in which their were observed. Localized structures can occur either in the presence [3] or in the absence [4] of a symmetry breaking instability. In the last case, bistability between uniform solutions is a prerequisite condition for LS formation. However, in the presence of a symmetry breaking instability, the coexistence between a single uniform solution and a patterned state allows for the stabilization of LSs [4]. In this case, bistability between uniform solutions is not a necessary condition for generating LSs [5].

Spatial coupling in many spatially extended systems is nonlocal. The kernel function that characterizes the nonlocality can be either weak and strong. If the kernel function decays asymptotically to infinity more slowly (faster) than an exponential function, the nonlocal coupling is said to be strong (weak) [6]. Self-organization phenomena leading to the formation of either extended or localized patterns under a local and nonlocal coupling occur in various systems such as fluid dynamics [7], firing of cells [8,9], propagation of infectious diseases [10], chemical reactions [11,12], population dynamics [13–15], nonlinear optics [16–22], and granular [23] and vegetation patterns [24–34].

We focus on the bistable regime far from any symmetry breaking instability, i.e., far from any Turing instability. In this case, the behavior of many systems is governed by the dynamics of front connection between the homogeneous states. When the nonlocal coupling is weak, the interaction between two fronts is usually described by the behavior of the tail of fronts. However, for strongly nonlocal coupling, the interaction is controlled by the whole kernel function and not by the asymptotic behavior of the front tails [6].

When a nonlocal coupling is weak, the asymptotic behavior of front solutions is characterized by exponential decay or damped oscillations. In the former case, front interaction is always attractive and decays exponentially with the distance between the fronts. In the case of damped oscillations, front interactions alternate between attractive and repulsive with an intensity that decays exponentially with the distance between the two fronts [35]. For a fixed value of parameters, a family of stable one-dimensional LSs with different sizes has been reported in [13,36–38]. When considering a strongly nonlocal coupling, the interaction between fronts can be repulsive [39,40].

Strongly nonlocal coupling has been observed experimentally in various systems. Indeed, several experimental measurements of nonlocal response in the form of Lorentzian or a generalized Lorentzian have been carried out in nematic liquid crystals cells [41,42]. Experimental reconstruction of strongly nonlocal coupling has also been performed in photorefractive materials [43]. In this case, the strongly nonlocal coupling is originating from the thermal medium effects. In population dynamics such as vegetation, it has been shown experimentally that seed dispersion may be described by a Lorentzian [44].

We consider a protomodel for population dynamics, namely the strongly nonlocal Nagumo equation [39]. This model possesses two relevant properties: strongly nonlocal coupling and bistability between uniformly vegetated and bare states. We focus on a regime far from any symmetry breaking or Turing-type instabilities. In this regime LSs resulting from strongly nonlocal coupling can be stabilized in a wide range of parameters [39]. We investigate two types of localized vegetation structures—(i) fairy circle (FC) and (ii) localized vegetation patch (LVP)—which correspond, respectively, to isolated or randomly distributed circular areas of barren

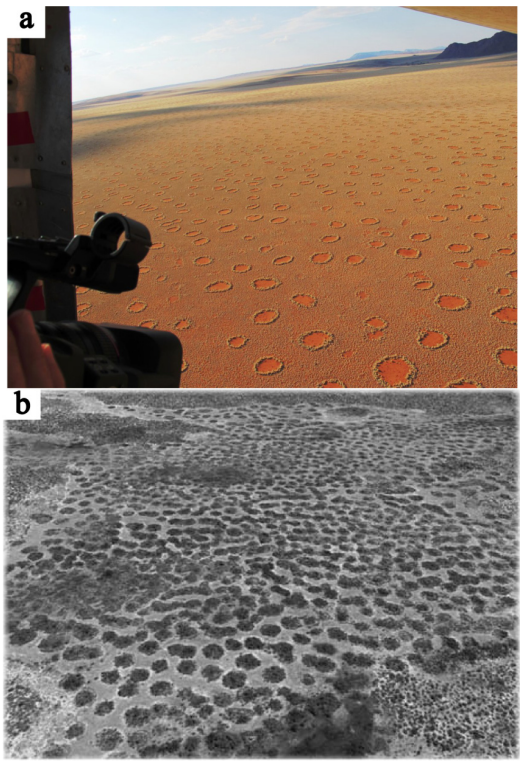

FIG. 1. (Color online) Localized vegetation patterns: (a) An aerial photo taken on 05 March 2010 shows fairy circles in the Namibrand region, Namibia. Image courtesy of Professor Norbert Juergens. (b) An aerial photograph showing LVPs, Zambia (taken from the review [29]).

patches of vegetation and circular areas of vegetation, surrounded by a bare region. An example of FCs is shown in an areal photograph [see Fig. 1(a)]. They are observed in vast territories in southern Angola, Namibia, and South Africa [45–53]. The size of these circles can reach diameters of up to 12 m. An in-depth investigation of several hypotheses concerning their origin has been performed by van Rooyen *et al.* [54]. In this study, these authors have been able to excluded the possible existence radioactive areas inapt for the development of plants, termite activity, and the release of allelopathic compounds. We attribute two main ingredients to their stabilization: the bistability between the bare state and the uniformly vegetation state, and the Lorentzian-like nonlocal coupling that models the competition between plants [40]. We provide detailed analysis of the FC formation in a simple population dynamics model. In addition, we show that the above mechanism applies to another type of LSs that consist of isolated or randomly distributed vegetation patches surrounded by a bare state. An example of this behavior is shown in Fig. 1(b). In this paper, we investigate analytically and numerically the formation of both FCs and localized patches and their existence ranges. Our theoretical analysis shows that there is a Maxwell point above which localized patches are stable, while below this point FCs appear. Finally, we investigate how the degree of aridity affects the widths of both types of localized vegetation structures.

This paper is organized as follows. After briefly introducing the model describing the vegetation dynamics, namely the Nagumo model with a strongly nonlocal coupling mediated by a Lorentzian function (Sec. II), we describe the dynamics of a single front in one dimension and its asymptotic behaviors (Sec. III). The analytical and the numerical analysis of the interaction between fronts connecting the uniformly vegetated and the bare steady states are described in Sec. IV, where we discuss the formation of both FCs and localized patches. Close to the Maxwell point, we derive a formula for the widths of both LSs as a function of the degree of the aridity in one dimension. We conclude in Sec. V.

II. THE NAGUMO MODEL

Several models describing vegetation patterns and self-organization in arid and semiarid landscapes have been proposed during past two decades. They can be classified into three types. The first approach is based on the relationship between the structure of individual plants and the facilitation-competition interactions existing within plant communities [24–26,55,56]. The second is based on a reaction-diffusion approach, which takes into account of the influence of water transport by below ground diffusion and/or above ground runoff [57–63]. The third approach focuses on the role of environmental randomness as a source of noise induced symmetry breaking transitions [29,64–66]. Recently, the reduction of a generic interaction-redistribution model, which belong to the first class of ecological-type models [26], to a Nagumo-type model has been established [40]. Here we consider the variational nonlocal Nagumo-type equation,

$$\partial_t u = u(\alpha - u)(u - 1) + \nabla^2 u + \epsilon u \int_\Omega u^2(\mathbf{r} + \mathbf{r}', t) K(\mathbf{r}') d\mathbf{r}', \tag{1}$$

where $u(\mathbf{r},t)$ is a normalized scalar field that represents the population density or biomass, $\alpha \in [0,1]$ is a parameter describing the environment adversity or the degree of aridity, t is time. We consider that population or plant community established on a spatially uniform territory Ω. The vegetation spatial propagation, via seed dispersion and/or other natural mechanisms, is usually modeled by a nonlocal coupling with a Gaussian-like kernel [24–26]. For simplicity, we consider only the first term in the Taylor expansion of the dispersion. This approximation leads to the Laplace operator, $\nabla^2 = \partial_{xx} + \partial_{yy}$ acting in the space $\mathbf{r} = (x,y)$. The last term in Eq. (1) describes the competitive interaction between individual plants through their roots. The nonlocal coupling intensity, denoted by ϵ, should be positive to ensure a competitive interaction between plants. The kernel function has the form $K(\mathbf{r}) = \delta(\mathbf{r}) - f_\sigma(\mathbf{r})$, where $\delta(\mathbf{r})$ is the Dirac δ function. The inclusion of the δ function in the analysis allows us to avoid the variation of the spatially uniform states as a function the nonlocal intensity ϵ, and

$$f_\sigma(\mathbf{r}) = \frac{N_n}{1 + (|\mathbf{r}|/\sigma)^n}, \tag{2}$$

which has an effective range σ. For the sake of simplicity, we consider that the length σ is a constant, independent of the biomass. Hence, we assume that all plants have the same root size; that is, we neglect allometric effect [55,67]. At large

distance, the asymptotic behavior of the kernel is determined by n, and N_n is normalization constant.

It is worth emphasizing that, since the strongly nonlocal term in Eq. (1) models the interaction between individual plants at the community level, we refer to it as strongly nonlocal interaction or coupling. In contrast, nonlocalities describing transport processes, such as seed dispersion [24–26], for sake of simplicity, we are modeling by the Laplace operator.

Equation (1) is variational and it is described by

$$\partial_t u = -\frac{\delta \mathcal{F}}{\delta u} \Rightarrow \frac{d\mathcal{F}}{dt} \leqslant 0, \tag{3}$$

where $\mathcal{F}$ is a Lyaponov functional that can only decrease in the course of time. Accordingly, any initial distribution $u(\vec{r},t)$ evolves towards a homogeneous or inhomogeneous (periodic or localized) state corresponding to a local or global minimum of $\mathcal{F}$. The Lyaponov functional reads

$$\mathcal{F}[u] = \int_\Omega \left\{ \frac{1}{2}(|\nabla u|^2 + V(u) \right\} dr + \frac{\epsilon}{4} \int_\Omega \int_\Omega u^2(\mathbf{r}) u^2(\mathbf{r}') K(\mathbf{r}-\mathbf{r}') dr dr'$$

and

$$V(u) = \frac{u^2}{4}(u-1)^2 + \frac{u^2}{6}(\alpha - 1/2)(3-2u). \tag{4}$$

Equation (1) admits three spatially uniform solutions: $u = 0, u = \alpha$, and $u = 1$. The bare state $u = 0$ is always stable and represents the non-plant state. The uniform state $u = \alpha$ is always unstable. For large values of α, the climate becomes more and more arid. The uniformly vegetated state $u = 1$ may undergo a symmetry breaking type of instability (often called Turing instability), which leads to pattern formation. In a one-dimensional system, and for $n = 2$, the threshold for that instability satisfies

$$\beta = \epsilon \sigma^2 \exp(-\beta), \tag{5}$$

with $\beta = \sqrt{1 + \sigma^2(2\epsilon + \alpha - 1)} - 1$. In what follows, we focus on a regime far from any pattern forming instability.

III. FRONTS

We consider a bistable regime where $u = 0$ and $u = 1$ are both linearly stable. From Eq. (4), $V(0) = 0$ and $V(1) = (\alpha - 1/2)/6$. Therefore, when $\alpha < 1/2$, the most favorable state is the uniformly vegetated one. When $\alpha > 1/2$, the bare state is more stable than the uniformly vegetated one. There exists a particular point where both states are equally stable. This point is usually called the Maxwell point [68] and corresponds to $\alpha = 1/2$.

Depending on the value of α, the front connecting both states will propagate towards the most stable state. An example of a single front is illustrated in Fig. 2(a). The time-space diagram of Fig. 2(b) shows how the most stable state, corresponding to the bare state ($\alpha > 1/2$), invades the uniformly vegetated state, with a constant speed. Fronts propagate following the minimization of the potential (4) and the front velocity is proportional to the energy difference between equilibria $V(1) - V(0)$. The front is motionless at

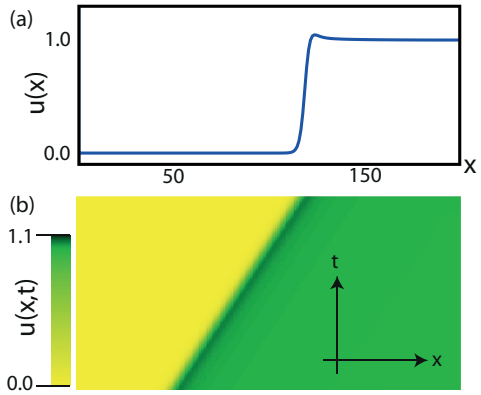

FIG. 2. (Color online) Front propagation obtained from numerical simulations of Eq. (1). (a) Biomass front profile. (b) Spatiotemporal diagram that shows the front movement with a constant speed. The parameters are $\alpha = 0.51$, $\sigma = 0.7$, $n = 2$, and $\epsilon = 1.0$.

the Maxwell point for $\alpha = 1/2$. At this point and in the absence of nonlocal coupling, $\epsilon = 0$, front solutions are written

$$u_\pm(x - x_0) = \frac{1}{2}\left[1 \pm \tanh\left(\frac{x - x_0}{2\sqrt{2}}\right)\right], \tag{6}$$

where x_0 corresponds to the interphase position. The front u_+ links the barren state from $x = -\infty$ to the uniformly vegetated state at $x = \infty$. The opposite connection corresponds to u_-.

The asymptotic behavior of front solution u_+ obeys an exponential law of the form

$$u_+(x \ll x_0) \approx e^{(x-x_0)/\sqrt{2}},$$
$$u_+(x \gg x_0) \approx 1 - e^{-(x-x_0)/\sqrt{2}}.$$

Around the barren state ($u = 0$), the inclusion of the nonlocal interaction does not modify the asymptotic behavior of the front, since the nonlocality in model (1) is nonlinear. Let us examine the effect of the nonlocal term around the uniformly vegetated state ($u = 1$). For this purpose, let us assume that the asymptotic behavior of the front obeys an exponential law of the form

$$u(x \gg x_0) \approx 1 - ce^{-\lambda(x-x_0)},$$

where c is a constant, and the exponent λ obeys the equation

$$\lambda^2 - \tfrac{1}{2} + \epsilon[3 - 2g_\sigma(\lambda)] = 0,$$

where

$$g_\sigma(\lambda) = \int_{-\infty}^{\infty} \cosh(\lambda x) f_\sigma(x) dx.$$

This equation has been successfully used to explain the emergence of localized domains. When λ solutions have a non-null imaginary part, spatially damped oscillations on the front profile are induced, leading to the stabilization of localized domain. This mechanism is well documented for either local or nonlocal systems [13,36,37,69].

The g_σ function exists when the kernel decays faster than an exponential one, i.e., a weakly nonlocal coupling. In the case of strongly nonlocal interaction, g_σ diverges and the above analysis is no more longer valid.

To determine the asymptotic behavior of the front around the uniformly vegetated state under a strongly nonlocal coupling, we perform a regular perturbation analysis in terms of small parameter ϵ. At the Maxwell point, we expand the field as

$$u(x) = u_0(x) + \epsilon u_1(x) + \epsilon^2 u_2(x) + \cdots, \tag{7}$$

where $u_0 = u_+$ is the motionless front provided by Eq. (6). Replacing (7) in Eq. (1) and making an expansion in series of ϵ, at order ϵ, we obtain

$$\{\partial_{xx} - 1/2 + 3u_0(1-u_0)\}u_1 = \left[u_0 \int_{-\infty}^{\infty} u_0^2(x+x')f_\sigma(x')dx' - u_0^3\right].$$

Let us focus in the region $x \gg x_0$, and, neglecting all exponential corrections coming from u_0, then we obtain

$$\{\partial_{xx} - 1/2\}u_1 = -\int_{x-x_0}^{\infty} f_\sigma(x')dx'. \tag{8}$$

Equation (8) is a linear inhomogeneous equation for the correction u_1. For strongly nonlocal coupling, the particular solution of Eq. (8) dominates over the homogeneous one,

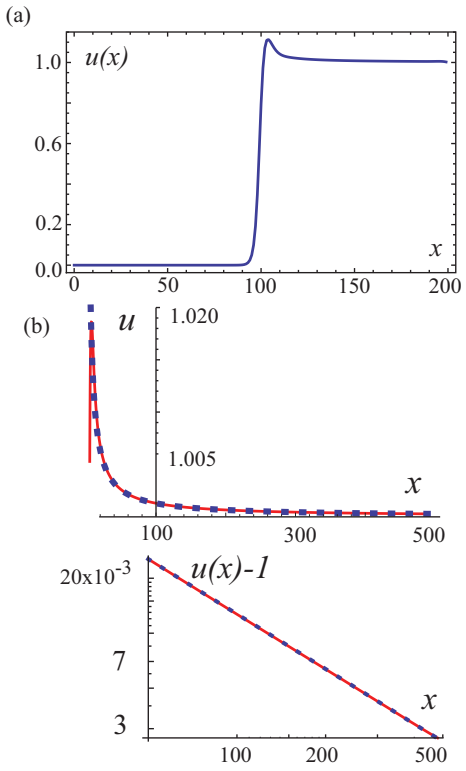

FIG. 3. (Color online) Numerical solutions of model (1) with the Lorentzian kernel (2). (a) Front profile at the Maxwell point $\alpha = 0.5$; other parameters are $\sigma = 2$, $n = 2$, and $\epsilon = 0.35$. (b) Decay of front to the uniformly vegetated state for $\alpha = 0.5$, $\sigma = 2$, $n = 2$, and $\epsilon = 0.1$. In (b), the top panel shows the comparison between the numerical calculation (dotted line) and the analytical estimation (10) (continuous line), while the bottom panel displays the same comparison in a log-log plot.

which is exponentially small, for instance, if we consider a kernel like

$$f_\sigma(x) \approx \frac{N}{x^n} \quad \text{for} \quad x \gg 1, \tag{9}$$

with $n > 1$ and N a normalization constant. For $x - x_0 \gg 1$, the front approaches asymptotically the following solution:

$$u \approx 1 + \frac{2\epsilon N}{(n-1)(x-x_0)^{n-1}}. \tag{10}$$

This solution decays according to a power law $1-n$. To check the power obtained from the above analysis, we perform numerical simulations of the full model Eq. (1). The result obtained from Eq. (9) and the numerical simulations are shown in Fig. 3. Both results agree perfectly without any adjusting parameter. Note that both analytical calculations and numerical simulations predict the existence of one peak in the spatial profile of the front. This peak takes place at the interface separating both homogeneous states as shown in Fig. 3.

IV. LOCALIZED VEGETATION PATTERNS

Far from a symmetry breaking instability, LSs can be stable as a results of front interactions. This phenomenon occurs when the spatial profile of the front exhibits damped oscillations [13,69]. However, around the bare state damped oscillations are nonphysical since the biomass is a positive defined quantity. A stabilization mechanism of LSs based on combined influence of strongly nonlocal coupling and bistability has been proposed [39]. This mechanism has been applied to explain the origin of the FC phenomenon in a realistic ecological model [40]. In addition, we have shown that the diameter of the single FC is intrinsic to the dynamics of the system, such as the competitive interaction between plant and the redistribution of resources [40]. We believe that extrinsic causes, such as termite or ant or others, cannot explain the circular shape of FCs.

In this section we provide a detailed analysis of front interactions leading to stabilization of both FCs and localized patches. For both types of localized vegetation structures, we discuss how the level of aridity affects their diameters.

A. Fairy circles

The model Eq. (1) admits stable LSs in the form of a bare state embedded in vegetated matrix. An example of such behavior is shown in Fig. 4. They are stable and permanent structures. A single FC exhibits a fringe formed by tall grass that separates the bare state from the uniformly vegetated as shown in Fig. 1(a). From numerical simulations, we see that the biomass possesses one peak that takes place in between the bare and the uniformly vegetated states as shown in Fig. 4. This can be explained by the fact that inside the circle the competition between plants is low. Indeed, the length of the plant root is much smaller than the diameter of the FC.

We analytically investigate the formation of a single FC in one spatial dimension. We focus on the parameter region near the Maxwell point ($\frac{1}{2} - \alpha = \eta \ll 1$) and consider a small nonlocal coupling ($\epsilon \ll 1$). We look for a solution of Eq. (1) that has the form of a slightly perturbed linear superposition

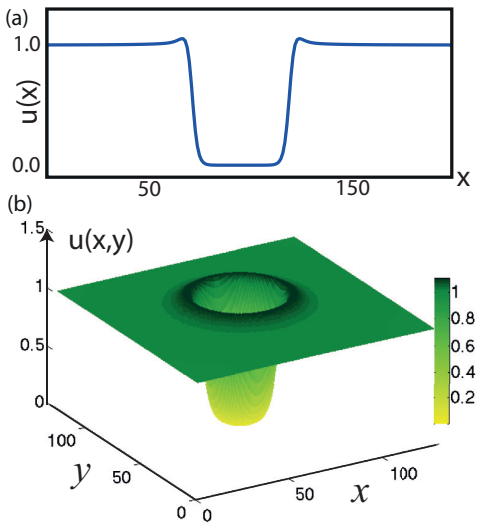

FIG. 4. (Color online) Stationary FC obtained from numerical simulations of Eq. (1). (a) One dimension with $\alpha = 0.492$, $\sigma = 0.8$, $n = 2$, and $\epsilon = 0.5$. (b) Two dimensions with $\alpha = 0.46$, $\sigma = 0.1$, $n = 2.5$, and $\epsilon = 10$.

of two fronts,

$$u(x,t) = u_+[x - \delta(t)] + u_-[x + \delta(t)] + W, \qquad (11)$$

where $W(x,u_+,u_-)$, $\partial_t\delta$, η, and ϵ are small in a sense that will be pinned down below, while $u_\pm$ are defined by Eq. (6).

Replacing ansatz (11) in Eq. (1) and neglecting high order terms in ϵ, we obtain

$$\begin{aligned} &-(\partial_x u_+ - \partial_x u_-)\partial_t\delta \\ &\quad = u_+u_-(3 - 3u_+ - 3u_-) \\ &\qquad + \epsilon u \int_{-\infty}^{\infty} u^2(x + x',t)K(x')dx' \\ &\qquad - \eta(u_+ + u_- - 1)(u_+ + u_-) + LW + \text{h.o.t.}, \end{aligned} \qquad (12)$$

where the linear operator L has the form

$$L \equiv -\tfrac{1}{2} + 3u_+ - 3u_+^2 + \partial_{xx} + 3u_- - 3u_-^2 - 6u_+u_-.$$

To solve the above equation, we consider the inner product $\langle g|h\rangle \equiv \int_{-\infty}^{+\infty}[g(x)h(x)]dx$. Then, the linear operator L_+ is self-adjoint and $L\partial_x u_\pm \approx 0$. The solvability condition gives

$$-\langle \partial_x u_+|\partial_x u_+\rangle\, \partial_t\delta = G + \eta\,\langle \partial_x u_+|(1 - u_+)u_+\rangle\,, \qquad (13)$$

where

$$G(u_\pm,\sigma) = \langle \partial_x u_+ \left| u_+ \int_{-\infty}^{\infty} u^2(x',t)K(x' - x)dx' \right\rangle.$$

We neglect also the terms smaller than $1/\delta^{2n-1}$ in Eq. (13). Then it is obtained

$$\partial_t\delta = \frac{3\sqrt{2}\epsilon N_n\sigma^n}{(n-1)(2\delta)^{n-1}} - \sqrt{2}\eta. \qquad (14)$$

Strictly speaking, this equation of motion is quantitatively valid when $\partial_t\delta \sim \epsilon/\delta^{n-1} \sim \eta \ll 1$.

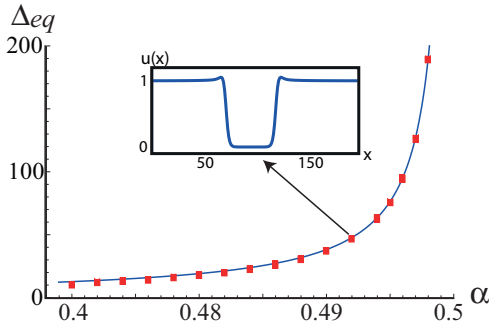

FIG. 5. (Color online) Width of a FC as a function of aridity α in one dimension. The solid line represents the analytical prediction from Eq. (16). The squares are obtained by numerical simulations of Eq. (1). The inset is the spatial profile of biomass. Parameters are $\sigma = 0.8$, $n = 2$, and $\epsilon = 0.5$.

This result is valid for any power $n > 1$ in the kernel function (2). We consider $n = 2$ and $N_n = 1/\pi\sigma$ in one dimension. Then Eq. (14) takes the form

$$\partial_t\Delta = \frac{6\sqrt{2}\epsilon\sigma}{\pi\Delta} - 2\sqrt{2}\left(\frac{1}{2} - \alpha\right), \qquad (15)$$

where $\Delta = 2\delta$ is the width of the LS. The equilibrium width is given by

$$\Delta_{\text{eq}} = \frac{3\epsilon\sigma}{\pi\left(\frac{1}{2} - \alpha\right)}. \qquad (16)$$

The linear stability analysis allows us to determine the eigenvalue $\lambda = -2\sqrt{2}\pi\eta^2/3\epsilon\sigma$. Therefore, for competitive interaction, i.e., $\epsilon > 0$, FCs are always stable.

We plot the width of the FC in one dimension as function of the aridity α in Fig. 5. The width of the LS grows as aridity increases. At the Maxwell point, i.e., $\alpha = 1/2$, the width of the FC becomes infinite. In order to check the approximations used to derive the equilibrium size (16), we perform numerical simulations of Eq. (1). Both results are in good agreement, without any fitting parameter.

The FCs are observed in vast territories in southern Angola, Namibia, and South Africa [46,47], where the annual rainfall ranges between 50 and 150 mm [54]. The size of a FC increases from south to north where the climate becomes more and more arid [54]. The size can also be affected by the rainfall and nutrients [48]. Fairy circle average diameter varies in the range of 2–12 m [54]. In agreement with field observations, Fig. 5 shows, indeed, that FC diameter increases with the aridity.

Therefore, one-dimensional front interaction explains why FC size increases with the aridity. To wit, as environment aridity increases, the bare state becomes more and more favorable, increasing FC size. This mechanism demands, however, that the uniformly vegetated state must be always the most favorable one ($\alpha < 1/2$); otherwise the bare state propagates indefinitely. The same tendency is observed in two-dimensional simulations [40].

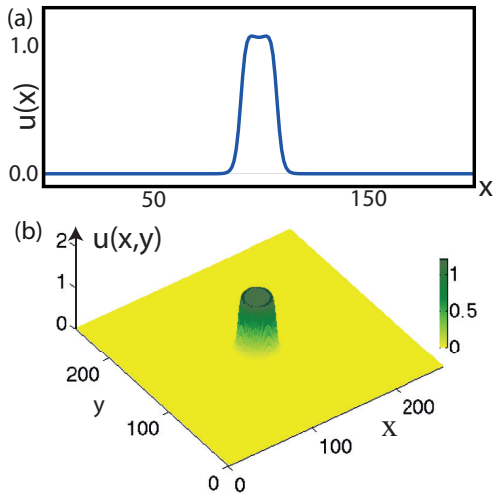

FIG. 6. (Color online) Stationary localized patch obtained from numerical simulations of Eq. (1). (a) One dimension with $\alpha = 0.52$, $\sigma = 0.8$, $n = 2$, and $\epsilon = 0.5$. (b) Two dimensions with $\alpha = 0.56$, $\sigma = 0.1$, $n = 2.5$, and $\epsilon = 10$.

B. Localized vegetation patch

In this section, we investigate the formation of a single localized patch that consists of a circular vegetated state surrounded by a bare state. This behavior occurs for high values of the aridity parameter, i.e., $\alpha > 1/2$. An example of a single localized patch is illustrated in Fig. 6. This localized solution corresponds to the counterpart of FCs.

Following a strategy similar to that in the previous section (small ϵ and $\eta_f = \alpha - 1/2$), the patch width Δ in one spatial dimension obeys

$$\partial_t \Delta = \frac{6\sqrt{2}\epsilon N_n \sigma^n}{(n-1)(\Delta)^{n-1}} - 2\sqrt{2}\eta_f. \tag{17}$$

Note that, like in Eq. (14), the result obtain in Eq. (17) is generic for any n in (2). For $n = 2$, the stable vegetated patch has the size

$$\Delta_{\rm eq} = \frac{3\epsilon\sigma}{\pi\left(\alpha - \frac{1}{2}\right)}. \tag{18}$$

The formula (18) is plotted in Fig. 7 by a solid line. Confrontation with direct numerical computation for the localized patch width is in good agreement, as shown in Fig. 7. There are no available data from the field observation to confirm this theoretical prediction.

C. Bifurcation diagram

In this section, we establish the bifurcation diagram for both types of localized vegetation structures. We fix the length of the completion between plants σ, and we vary the degree of aridity α and the strength of the competitive interaction ϵ. We numerically establish a stability range of a single FC and the localized patch in a one-dimensional setting. This analysis is summarized in the parameter plane (α,ϵ) of Fig. 8. For $\alpha < 1/2$, a single FC is stable in the region FC, as indicated in Fig. 8. This stability region is bounded from

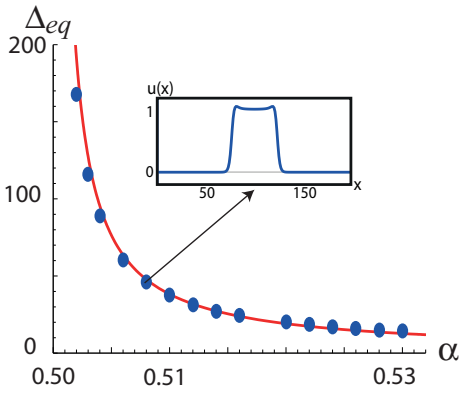

FIG. 7. (Color online) Width of a LVP, as a function of aridity α in one dimension. The solid line represents the analytical prediction from Eq. (18). The dots are obtained by numerical simulations of Eq. (1). The inset is the spatial profile of biomass. Parameters are $\sigma = 0.8$, $n = 2$, and $\epsilon = 0.5$.

below by dots and bounded from the left by the Maxwell point ($\alpha = 1/2$). Dynamically speaking, dots correspond to a saddle-node bifurcation. The parameter zone A indicates the regime where a FC shrinks and disappears. For large values of the strength of the competition ϵ, the uniformly vegetated state becomes unstable via a pattern-formimg instability. The threshold associated with this instability is represented by a solid line. This line is obtained by plotting formula Eq. (5). This spatial instability impedes the existence of FCs in the region C and may allow for the formation of periodic structures. For $\alpha > 1/2$, a single FC grows *ad infinitum* and disappears and a LVP appears. This structure is stable in the region LVP, as shown in the bifurcation diagram of Fig. 8. The region B corresponds to a high degree of aridity. In this zone of parameters, a localized patch shrinks and disappears, and the transition toward a bare state occurs.

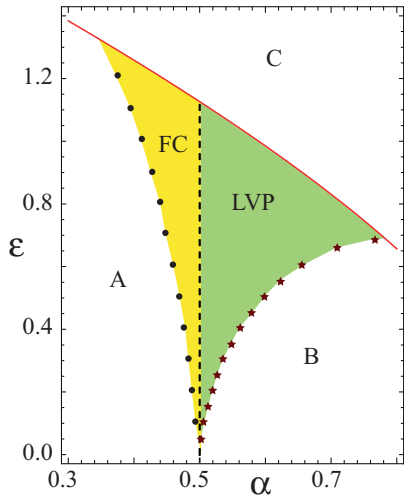

FIG. 8. (Color online) Bifurcation diagram of LSs for model Eq. (1), in parameter plane (α,ϵ), with $\sigma = 0.8$ and $n = 2$.

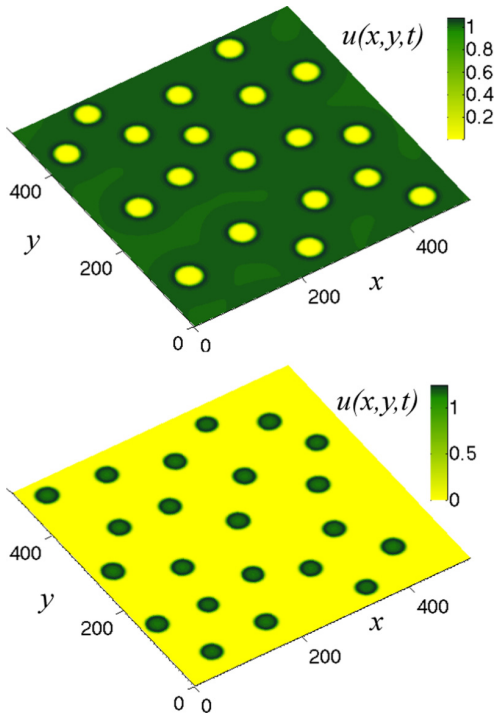

FIG. 9. (Color online) Two-dimensional localized vegetation patterns obtained from numerical simulations of Eq. (1). (a) Multi-FCs for $\alpha = 0.44$; (b) multi-LVPs for $\alpha = 0.57$. Other parameters are $\sigma = 0.1$, $\epsilon = 10$, and $n = 2.5$.

V. CONCLUSIONS

We have investigated the role of a strongly nonlocal coupling in a bistable model, namely the Nagumo model. This prototype model of population dynamics could be applied to vegetation dynamics. We have shown that, far from any symmetry breaking or Turing-type instability, localized vegetation structures can be stabilized in large values of the aridity parameter. Their formation is attributed to the interaction between fronts mediated by a strongly nonlocal coupling in the form of a Lorentzian. We have identified the following scenario. When increasing the level of the aridity, a large dip embedded in a uniformly vegetated state is formed. This structure has a single fringe peak that appears in the spatial profile of the biomass. We have interpreted this behavior as a FC. When increasing further the degree of aridity, LVPs can be formed in the system. These structures have a peak surrounded by the bare state.

The LSs reported in this work have varying widths as a function of aridity. In contrast, the widths of localized vegetation structures found close to the symmetry breaking instability are determined by the most unstable Turing wavelength [26,70]. We have established analytically a formula for the widths of FCs and LVPs as functions of the degree of aridity. The widths of these LSs are intrinsic to the dynamics of arid ecosystems and are independent of external environmental effects, such as termites or ants. The results of direct numerical simulations of model Eq. (1) agreed with the analytical findings.

In this paper we have focused our analysis on a single LS; several of them could be stable, as shown in the Fig. 9. The formation of multiple dips or peaks LSs, their interactions, and their stability are under investigation. Understanding the formation of LSs is central not only in arid ecosystems but also in spatially extended out of equilibrium systems.

ACKNOWLEDGMENTS

M.G.C. acknowledges the financial support of FONDECYT Project No. 1120320. D.E. acknowledges the financial support of FONDECYT Project No. 1140128. C.F.-O. acknowledges the financial support of Becas Chile. M.T. received support from the Fonds National de la Recherche Scientifique (Belgium).

[1] H. Leblond and D. Mihalache, Phys. Rep. **523**, 61 (2013).

[2] M. Tlidi, K. Staliunas, K. Panajotov, A. G. Vladimiorv, and M. G. Clerc, Phil. Trans. R. Soc., A **372**, 20140101 (2014).

[3] Y. Pomeau, Phys. D **23**, 3 (1986); M. Tlidi, P. Mandel, and R. Lefever, Phys. Rev. Lett. **73**, 640 (1994); P. Coullet, C. Riera, and C. Tresser, Prog. Theor. Phys. Suppl. **139**, 46 (2000); M. G. Clerc and C. Falcon, Phys. A **356**, 48 (2005); U. Bortolozzo, M. G. Clerc, C. Falcon, S. Residori, and R. Rojas, Phys. Rev. Lett. **96**, 214501 (2006); M. G. Clerc, E. Tirapegui, and M. Trejo, *ibid.* **97**, 176102 (2006); M. Tlidi and L. Gelens, Opt. Lett. **35**, 306 (2010); A. G. Vladimirov, R. Lefever, and M. Tlidi, Phys. Rev. A **84**, 043848 (2011); V. Skarka, N. B. Aleksic, M. Lekic, B. N. Aleksic, B. A. Malomed, D. Mihalache, and H. Leblond, *ibid.* **90**, 023845 (2014).

[4] K. Staliunas and V. J. Sanchez-Morcillo, Phys. Lett. A **241**, 28 (1998); M. Tlidi, P. Mandel, and R. Lefever, Phys. Rev. Lett. **81**, 979 (1998); H. Calisto, M. Clerc, R. Rojas, and E. Tirapegui, *ibid.* **85**, 3805 (2000); M. Tlidi, P. Mandel, M. Le Berre, E. Ressayre, A. Tallet, and L. Di Menza, Opt. Lett. **25**, 487 (2000); D. Gomila, P. Colet, G. L. Oppo, and M. San Miguel, Phys. Rev. Lett. **87**, 194101 (2001); C. Chevallard, M. Clerc, P. Coullet, and J.-M. Gilli, Europhys. Lett. **58**, 686 (2002).

[5] U. Bortolozzo, M. G. Clerc, and S. Residori, New J. Phys. **11**, 093037 (2009).

[6] D. Escaff, Eur. Phys. J. D **62**, 33 (2011).

[7] P. Kolodner, D. Bensimon, and C. M. Surko, Phys. Rev. Lett. **60**, 1723 (1988); O. Thual and S. Fauve, J. Phys. (Paris) **49**, 1829 (1988); B. A. Malomed and A. A. Nepomnyashchy, Phys. Rev. A **42**, 6009 (1990); W. Barten, M. Lücke, and M. Kamps, Phys. Rev. Lett. **66**, 2621 (1991); H. Riecke, *ibid.* **68**, 301 (1992); M. Dennin, G. Ahlers, and D. S. Cannell, Science **272**, 388 (1996); P. B. Umbanhowar, F. Melo, and H. L. Swinney, Nature (London) **382**, 793 (1996); H. Riecke and G. D. Granzow, Phys. Rev. Lett. **81**, 333 (1998); C. Crawford and H. Riecke, Phys. D (Amsterdam, Neth.) **129**, 83 (1999).

[8] E. Hernandez-Garcia and C. Lopez, Phys. D (Amsterdam, Neth.) **199**, 223 (2004).

[9] J. D. Murray, *Mathematical Biology* (Springer-Verlag, Berlin, 1989).

[10] S. Ruan, in *Mathematics for Life Science and Medicine Biological and Medical Physics*, edited by Y. Takeuchi, Y. Iwasa, and K. Sato (Springer, Berlin, 2007).

[11] Y. Kuramoto, D. Battogtokh, and H. Nakao, Phys. Rev. Lett. **81**, 3543 (1998).

[12] S. I. Shima and Y. Kuramoto, Phys. Rev. E **69**, 036213 (2004).

[13] M. G. Clerc, D. Escaff, and V. M. Kenkre, Phys. Rev. E **72**, 056217 (2005); **82**, 036210 (2010).

[14] D. Escaff, Int. J. Bifurcation Chaos Appl. Sci. Eng. **19**, 3509 (2009).

[15] M. Hernandez, D. Escaff, and R. Finger, Phys. Rev. E **85**, 056218 (2012).

[16] W. Krolikowski and O. Bang, Phys. Rev. E **63**, 016610 (2000).

[17] W. Krolikowski, O. Bang, J. J. Rasmussen, and J. Wyller, Phys. Rev. E **64**, 016612 (2001).

[18] O. Bang, W. Krolikowski, J. Wyller, and J. J. Rasmussen, Phys. Rev. E **66**, 046619 (2002).

[19] Y. V. Kartashov, L. Torner, V. A. Vysloukh, and D. Mihalache, Opt. Lett. **31**, 1483 (2006).

[20] D. Mihalache, D. Mazilu, F. Lederer, L. C. Crasovan, Y. V. Kartashov, L. Torner, and B. A. Malomed, Phys. Rev. E **74**, 066614 (2006).

[21] Y. J. He, B. A. Malomed, D. Mihalache, and H. Z. Wang, Phys. Rev. A **77**, 043826 (2008).

[22] L. Gelens, G. Van der Sande, P. Tassin, M. Tlidi, P. Kockaert, D. Gomila, I. Veretennicoff, and J. Danckaert, Phys. Rev. A **75**, 063812 (2007).

[23] I. Aranson and L. Tsimring, *Granular Patterns* (Oxford University Press, New York, 2009).

[24] R. Lefever and O. Lejeune, Bull. Math. Biol. **59**, 263 (1997).

[25] O. Lejeune and M. Tlidi, J. Veg. Sci. **10**, 201 (1999).

[26] M. Tlidi, R. Lefever, and A. Vladimirov, in *Dissipative Solitons: From Optics to Biology and Medicine*, edited by N. Akhmediev and A. Ankiewicz, Lecture Notes in Physics Vol. 751 (Springer, Berlin, 2008), p. 381.

[27] E. Gilad, J. von Hardenberg, A. Provenzale, M. Shachak, and E. Meron, Phys. Rev. Lett. **93**, 098105 (2004).

[28] P. Couteron, F. Anthelme, M. G. Clerc, D. Escaff, C. Fernandez-Oto, and M. Tlidi, Phil. Trans. R. Soc., A **372**, 20140102 (2014).

[29] F. Borgogno, P. D'Odorico, F. Laio, and L. Ridolfi, Rev. Geophys. **47**, RG1005 (2009).

[30] O. Lejeune, M. Tlidi, and P. Couteron, Phys. Rev. E **66**, 010901 (2002).

[31] M. Rietkerk, S. C. Dekke, P. C. de Ruiter, and J. van de Koppel, Science **305**, 1926 (2004).

[32] E. Meron, E. Gilad, J. von Hardenberg, M. Shachak, and Y. Zarmi, Chaos, Solitons Fractals **19**, 367 (2004).

[33] E. Meron, H. Yizhaq, and E. Gilad, Chaos **17**, 037109 (2007).

[34] E. Sheffera, H. Yizhaqa, M. Shachaka, and E. Meron, J. Theor. Biol. **273**, 138 (2011).

[35] W. van Saarloos and P. C. Hohenberg, Phys. D **56**, 303 (1992).

[36] L. Gelens, D. Gomila, G. Van der Sande, M. A. Matías, and P. Colet, Phys. Rev. Lett. **104**, 154101 (2010).

[37] P. Colet, M. A. Matías, L. Gelens, and D. Gomila, Phys. Rev. E **89**, 012914 (2014).

[38] L. Gelens, M. A. Matías, D. Gomila, T. Dorissen, and P. Colet, Phys. Rev. E **89**, 012915 (2014).

[39] C. Fernandez-Oto, M. G. Clerc, D. Escaff, and M. Tlidi, Phys. Rev. Lett. **110**, 174101 (2013).

[40] C. Fernandez-Oto, M. Tlidi, D. Escaff, and M. G. Clerc, Phil. Trans. R. Soc., A **372**, 20140009 (2014).

[41] X. Hutsebaut, C. Cambournac, M. Haelterman, J. Beeckman, and K. Neyts, J. Opt. Soc. Am. B **22**, 1424 (2005).

[42] J. F. Henninot, J. F. Blach, and M. Warenghem, J. Opt. A **9**, 20 (2007).

[43] A. Minovich, D. N. Neshev, A. Dreischuh, W. Krolikowski, and Y. S. Kivshar, Opt. Lett. **32**, 1599 (2007).

[44] H. F. Howe and L. C. Westley, *Plant Ecology*, 2nd ed. (Wiley, New York, 1986), Chap. 9.

[45] L. Fraley, Environ. Exp. Bot. **27**, 193 (1987).

[46] C. F. Albrecht, J. J. Joubert, and P. H. De Rycke, S. Afr. J. Sci. **97**, 23 (2001).

[47] T. Becker and S. Getzin, Basic Appl. Ecol. **1**, 149 (2000).

[48] M. D. Cramer and N. N. Barge, PLoS ONE **8**, e70876 (2013).

[49] M. D. Picker, V. Ross-Gillespie, K. Vlieghe, and E. Moll, Ecol. Entomol. **37**, 33 (2012).

[50] W. J. Jankowitz, M. W. Van Rooyen, D. Shaw, J. S. Kaumba, and N. van Rooyen, S Afr. J. Bot. **74**, 332 (2008).

[51] Y. Naude, M. W. van Rooyen, and E. R. Rohwer, J. Arid Environ. **75**, 446 (2011).

[52] N. Juergens, Science **339**, 1618 (2013).

[53] S. Grube>, Basic Appl. Ecol. **3**, 367 (2002).

[54] M. W. van Rooyen, G. K. Theron, N. van Royen, W. J. Jankowitz, and W. K. Matthews, J. Arid Environ. **57**, 467 (2004).

[55] R. Lefever and J. W. Turner, C. R. Méc. **340**, 818 (2012).

[56] R. Martínez-García, J. M. Calabrese, E. Hernandez-Garcia, and C. Lopez, Geophys. Res. Lett. **40**, 6143 (2013).

[57] C. A. Klausmeier, Science **284**, 1826 (1999).

[58] J. von Hardenberg, E. Meron, M. Shachak, and Y. Zarmi, Phys. Rev. Lett. **87**, 198101 (2001).

[59] R. HilleRisLambers, M. Rietkerk, F. van den Bosch, H. H. T. Prins, and H. de Kroon, Ecology **82**, 50 (2001).

[60] T. Okayasu and Y. Aizawa, Prog. Theor. Phys. **106**, 705 (2001).

[61] J. A. Sherratt, J. Math. Biol. **51**, 183 (2005).

[62] W. Wang, Q.-X. Liu, and Z. Jin, Phys. Rev. E **75**, 051913 (2007).

[63] S. Kefia, M. Rietkerka, M. van Baalenb, and M. Loreauc, Theor. Popul. Biol. **71**, 367 (2007).

[64] P. D'Odorico, F. Laio, and L. Ridolfi, J. Geophys. Res. **111**, G03010 (2006).

[65] P. D'Odorico, F. Laio, A. Porporato, L. Ridolfi, and N. Barbier, J. Geophys. Res. **112**, G02021 (2007).

[66] L. Ridif, P. D'Odorici, and F. Laio, *Noise Induced Phenomena in the Environmental Sciences* (Cambridge University Press, Cambridge, UK, 2011).

[67] R. Lefever, N. Barbier, P. Couteron, and O. Lejeune, J. Theor. Biol. **261**, 194 (2009).

[68] R. E. Goldstein, G. H. Gunaratne, L. Gil, and P. Coullet, Phys. Rev. A **43**, 6700 (1991).

[69] P. Coullet, Int. J. Bifurcation Chaos Appl. Sci. Eng. **12**, 2445 (2002).

[70] S. Getzin, K. Wiegand, T. Wiegand, H. Yizhaq, J. von Hardenberg, and E. Meron, Ecography **37**, 001 (2014).